RSC Advances

ROYAL SOCIETY OF CHEMISTRY

www.rsc.org/advances

Flexible cage-like carbon spheres with ordered mesoporous structures prepared *via* soft-template/hydrothermal process from carboxymethylcellulose

Qiong Wu, Wei Li, Jia Tan and Shouxin Liu*

[a]*College of Materials Science and Engineering, Northeast Forestry University, Harbin 150040, China*

*Tel./fax: 86-451-82191204.

E-mail address: liushouxin@126.com (S.X. Liu)

Abstract

Novel carbon microspheres with tunable mesoporous structures and surface morphologies (CSF_n) were synthesized *via* hydrothermal carbonization using carboxymethylcellulose (CMC) as carbon source and the triblock copolymer Pluronic F127 as a soft template. The obtained carbon microspheres changed from smooth spheres when no F127 was added to walnut-like, strawberry-like, and cage-like structures when 0.5, 0.7, and 1.0 g, respectively, of F127 were added. Linear polymerization and cycloaddition of F127 with the CMC hydrothermal carbonized intermediate products enabled formation of carbon skeletons with higher thermal stabilities. After carbonization, the F127 in the carbon skeleton decomposed, leading to mesopore formation. In addition to the morphology, the mesoporous structure and specific surface area of the carbon microspheres can also be controlled by varying the mass of F127, the pore structure changed from stripe-like 2-D hexagonal mesostructure to cubic mesoporous to disordered worm-like pores. The unique ordered mesoporous structure resulted in the carbon spheres exhibiting high adsorption capacity for Vitamin B_{12}.

Key words: cage-like spheres; soft template; hydrothermal; mesoporous carbon

1. Introduction

Carbon materials with controllable sizes and morphologies are highly promising for various applications such as catalysts [1], adsorbents [2], super-capacitors [3], fuel cells, and electrode materials [4–5]. Spherical carbon materials (CSs) have great potential because of their high specific surfaces, low densities, and good electrical and heat conduction properties. Recent studies have shown that CSs can be obtained *via* hydrothermal treatment of monosaccharides, cellulose, and biomass, and this is a promising direction for the preparation of spherical carbon materials [6,7].

Many approaches have been developed for preparing CSs with controllable surface properties and ordered pore structures [8-9], because the rigid and uniform structures significantly influence the chemical and physical behaviors of the obtained carbon materials. An effective method is the soft-template strategy, which involves the use of an amphiphilic block copolymer such as F127 [10], P123 [11], and a mixture of F127 and P123 [12] as structure-directing agents; the inorganic

carbon precursor can interact with surfactants *via* hydrogen bonds or coulombic forces, enabling the formation of primary particles with different morphologies by cooperative self-assembly. This method avoids the complex synthetic routes of hard-template methods, and is used widely in the synthesis of spherical [13], sheet [14], rod [15], coral-like [16], and membrane [17] carbonaceous materials. After removal of the template at high temperature, 1D channels, 2D hexagons, and 3D cage-like ordered mesoporous structures can be controllably prepared. Yang and Wang [18] prepared hollow carbon nanoparticles of controllable size and morphology by hydrothermal treatment of α-cyclodextrin in the presence of Pluronic F127. Kube [16] prepared coral-like nanoarchitectured carbon monoliths with 3D continuous carbon branch networks *via* a one-pot, dual block copolymer–latex templating approach. The soft template plays a triple role in the formation of inverse opal pores, ordered microporous carbon walls, and micrometer-sized 3D continuous voids.

Sodium carboxymethylcelluloses (CMCs) are water-soluble ionic cellulose ethers; they exist in aqueous solutions as suspensions or emulsions, which means they can react in homogeneous systems during hydrothermal treatment. It is also possible to avoid the pyrolytic effect of the crystallinity of common cellulose [19-20], therefore CMCs are ideal precursors for the preparation of carbon materials by hydrothermal carbonization.

Here, we report the synthesis of spherical carbons with tunable surface morphologies and developed mesoporous structures, using CMC as the carbon source and F127 as a soft template. The morphology and mesoporous structure can be controlled obtained by adjusting the added mass of F127. The roles of F127 in the formation of cage-like carbon spheres with ordered mesoporous structures and their performance in the adsorption of VB_{12} was investigated systematically.

2. Experimental

2.1 Preparation of CSF_n

In a typical experiment, F127 (X g; X = 0.5, 0.7, 1.0, and 1.5) was dissolved in distilled water (40 mL), with heating at 60 °C in a water bath. Then, CMC (1.0 g) was added and the mixture was ultrasonically agitated for 15 min. The solution was poured into a stainless-steel autoclave (volume 55 mL). The autoclave was placed in a furnace at 210 °C for 12 h, and then allowed to

cool to room temperature. The black solid products were collected by filtration, washed with distilled water and pure ethanol until the solution ran clear, and vacuum dried at 80 °C for 12 h. The dried products were further carbonized in a tube furnace under N_2 at 800 °C for 2 h. The final products were referred to as CSF_n, where *n* denotes the mass of F127 added; materials without addition of F127, referred to as CSs, were used for comparison, those without carbonization were referred to as CSF_{npre} and CSs_{pre}.

2.2 Characterization

The morphologies and sizes of the products were observed using environmental scanning electron microscopy (SEM; Quanta 200; FEI, Hillsboro, OR, USA). Transmission electron microscopy (TEM) images were obtained using a JEOL 2011 instrument (FEI, the Netherlands). The porous structure was characterized using N_2 adsorption–desorption isotherms at -196 °C, using an ASAP 2020 Micromeritics instrument. Prior to gas adsorption measurements, the carbon was degassed at 200 °C under vacuum for 4 h. The Brunauer–Emmett–Teller (BET) surface area was calculated from the N_2 adsorption isotherms using the BET equation. Solid-state cross-polarization/magic angle spinning (CP/MAS) ^{13}C NMR spectra were recorded at room temperature, using a Bruker Avance III 500 spectrometer (Bruker Biospin AG, Fallanden, Switzerland), at a MAS rate of 5 kHz, a contact time of 2 ms, and a frequency of 125.73 MHz. Fourier-transfer infrared (FTIR) spectra were recorded using an FTIR instrument (Perkin Elmer TV 1900, Waltham, MA, USA) in the range of 400–4000 cm^{-1}, with a resolution of 4 cm^{-1}. Thermogravimetric analysis (TGA) was performed using a Pyris1 TGA apparatus (Perkin Elmer, USA), at a heating rate of 20 °C min^{-1} under a N_2 flow rate of 20 mL min^{-1}.

2.3 Adsorption test for Vitamin B_{12}

In typical adsorption experiments, 1000 mg L^{-1} solutions of Vitamin B_{12} were prepared in deionized water. The solutions were diluted from 20 to 200 mg L^{-1} for further use.

The prepared carbon sample (0.01 g) was suspended in solutions (10 mL) containing different concentrations of Vitamin B_{12}. Each mixture was then shaken at 30 °C for 24 h at a frequency of 150 strokes min^{-1}. The suspensions were filtered through 0.45-μm membrane filters. The amounts of Vitamin B_{12} left in solution were detected using UV spectrophotometer at 361 nm (TU-1900, Beijing).

3. Results and discussion

3.1 SEM and TEM analysis

SEM images of CSs, $CSF_{0.5}$, $CSF_{0.7}$, and $CSF_{1.0}$ are presented in Fig. 1 (a-d). It can be seen that spherical CSs (diameter 1–4 μm) with smooth outer surfaces were formed when no F127 was added (Fig. 1a). Figure 1b–d shows that the size and morphology of the carbon spheres can be controlled by changing the mass of F127. $CSF_{0.5}$ (Fig. 1b-I, b-II) showed walnut-like spherical structures with diameters increased to nearly 4–6 μm. When the mass of F127 was increased to 0.7 g, the size and regularity were nearly the same, but the obtained carbon spheres (Fig. 1c) showed strawberry-like structures, which consisted of many small spheres with size of tens nanometers. When the mass of F127 was increased further, the product, $CSF_{1.0}$, had an excellent cage-like carbon structure (diameter 5–8 μm) and the diameters of the small spheres increased to a few hundred nanometers.

F127 is a block polymer, and has amphiphilic properties; the hydrophilic groups [poly(ethylene oxide), PEO] can interact with monosaccharide hydroxyl groups *via* hydrogen bonds, enabling formation of spherical vesicles by cooperative self-assembly; the hydrophobic cores [poly(propylene oxide), PPO] provide ideal locations for encapsulation [21,22]. Dehydration, polymerization, and carbonization occur during hydrothermal carbonization of CMC, and various intermediate products such as aldehydes, ketones, and furans with reactive functional groups on their surfaces are generated [23,24]. The small vesicles begin as F127 cores in the CMC matrix and form spherical primary particles. The particles grow by constantly reacting with CMC, and the hydrothermal intermediate products are encapsulated in and around the vesicles during hydrothermal treatment.

For $CSF_{0.5}$, because the concentration of F127 is relatively low, it is difficult for F127 to self-assemble to give particular regular morphologies, and there is only an etching effect on the surface. At the same time, polymerization, decarbonylation, and aromatization occur between adjacent spherical primary particles *via* hydrogen bonds and reactive functional groups on their surfaces, as well as with reactive macromolecules [6,7,25], and spherical aggregates consisting of primary particles are produced.

Transmission electron microscopy (TEM) images of obtained CSs and CFS_n are shown in Fig.

1 e, it can be seen that F127 percentage had direct effects on the porous structure. CSs exhibited typical disordered worm-like pores, the high-resolution image shows that $CSF_{0.5}$ have long range ordered arrays in large domains, indicating the formation of stripe-like 2-D hexagonal mesostructure [26] [27]. As F127 increased to 1.0 g, another well-ordered array appeared, corresponding to cubic mesostructure [27-28], while disordered worm-like pores with some short range ordered structure appeared occasionally can be observed for $CSF_{1.5}$ (Fig. e-IV). In addition to reactions between F127 micellar structures and oxygen-containing carbonaceous precursors, assembly of the hydrophobic parts also contributes to the formation of mesoporous structures [29–32]. Carbonization of the material leads to opening of the pores and condensation of the carbon polymer skeleton, leading to the generation of different morphology of ordered mesoporous structure [33].

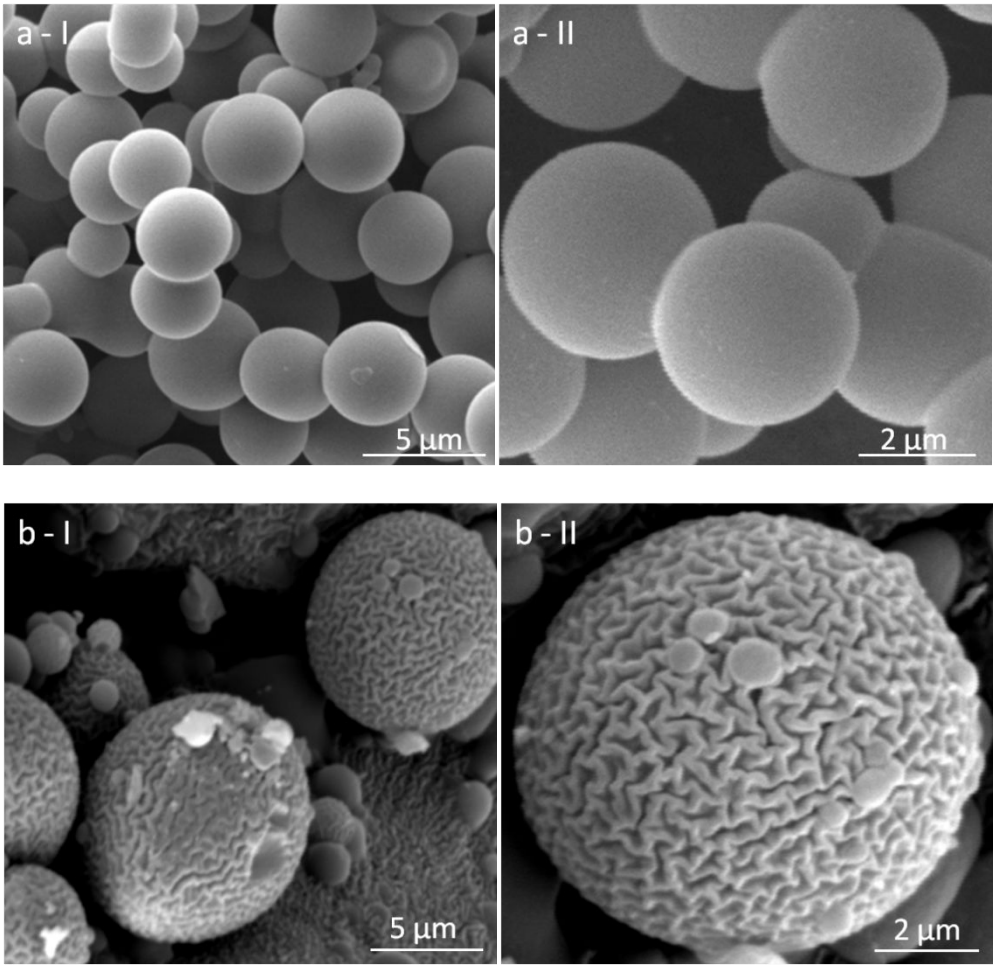

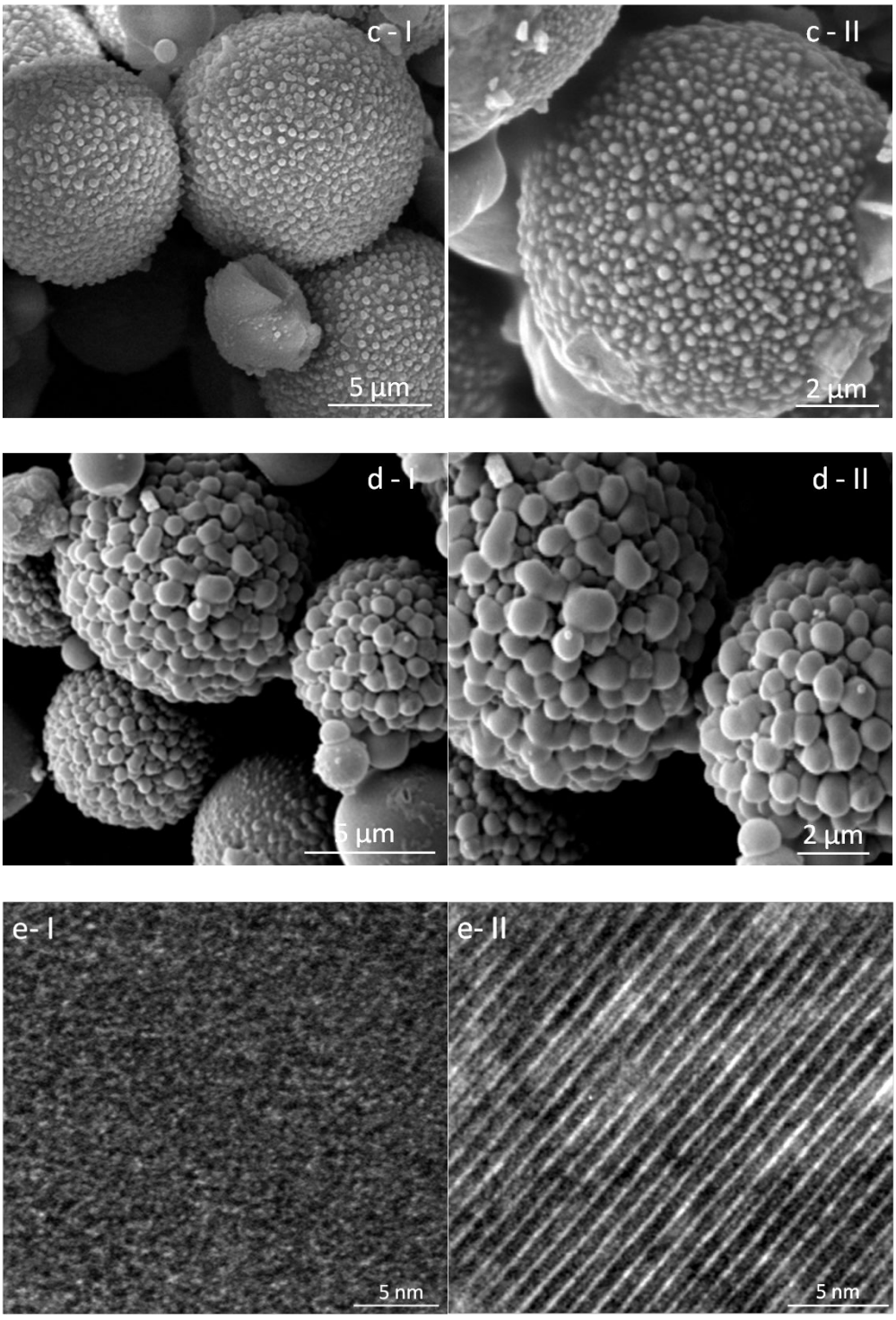

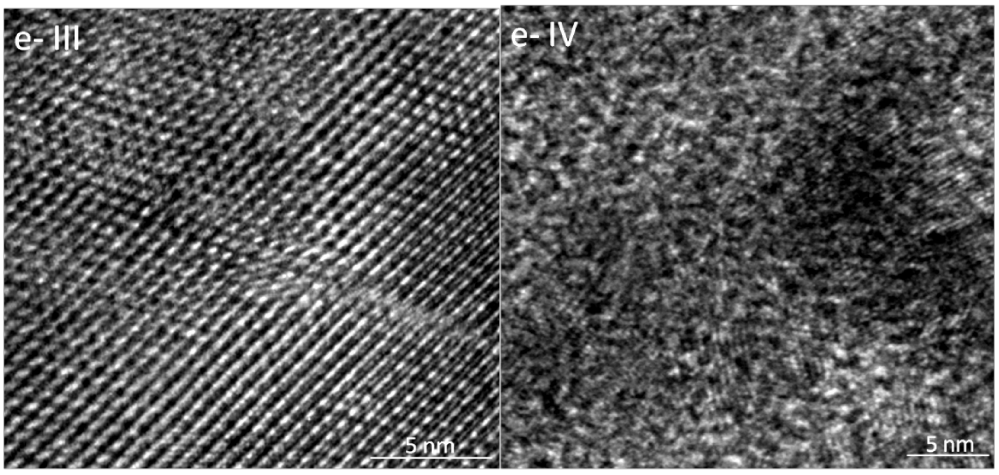

Fig.1 SEM images of CSs (a), $CSF_{0.5}$-800 (b), $CSF_{0.7}$-800 (c), $CSF_{1.0}$-800 (d) and TEM images of CSs (e-I), $CSF_{0.5}$ (e-II), $CSF_{1.0}$ (e- III), $CSF_{1.5}$ (e-IV)

3.2 Pore structure analysis

Figure 2 shows the N_2 adsorption–desorption isotherms for CSs, $CSF_{0.5}$, $CSF_{1.0}$, and $CSF_{1.5}$. All the samples exhibit type IV isotherms, with steep increases in the adsorption–desorption curves ($P/P_0 < 0.4$) and type H_2 hysteresis loops at higher pressures ($P/P_0 = 0.4–1.0$); this is associated with capillary condensation in the mesopores [34,35]. The shape and area of the hysteresis loop clearly change with increasing amount of F127, indicating that F127 directly influences mesopore generation.

As the data in Table 1 show, the CSs have a high specific surface area of 362.9 m^2/g, consisting of developed micropores; mesopores account for only 32.8% of the surface area. On addition of F127, the area of the hysteresis loop increased significantly. For $CSF_{0.5}$, the specific surface area is 385.6 m^2/g. The hysteresis loop is largest for $CSF_{1.0}$, and the percentage of the surface consisting of mesopores is 47.5%; this confirms that F127 can act as a porogen in the carbon structure, especially for mesopore generation. In the case of $CSF_{1.5}$, abundant micropores are generated, leading to the highest surface area, 410.5 m^2/g, with only 29.9% mesopores. It can be concluded that F127 acts as a pore-forming agent, and an appropriate amount of F127 is essential for mesopore generation. A high mass of F127 is conducive to micropore generation. The pore size distribution curves, calculated from the adsorption branch based on the BJH method, showed a uniform mesopores centered at 3.5 nm (Fig.2b), indicating that a large component and groups decomposed with carbonization led to pore structures shrinkage to 3.5 nm, more

concentrate until pore size distribution became uniform gradually, which was consistence with TEM result.

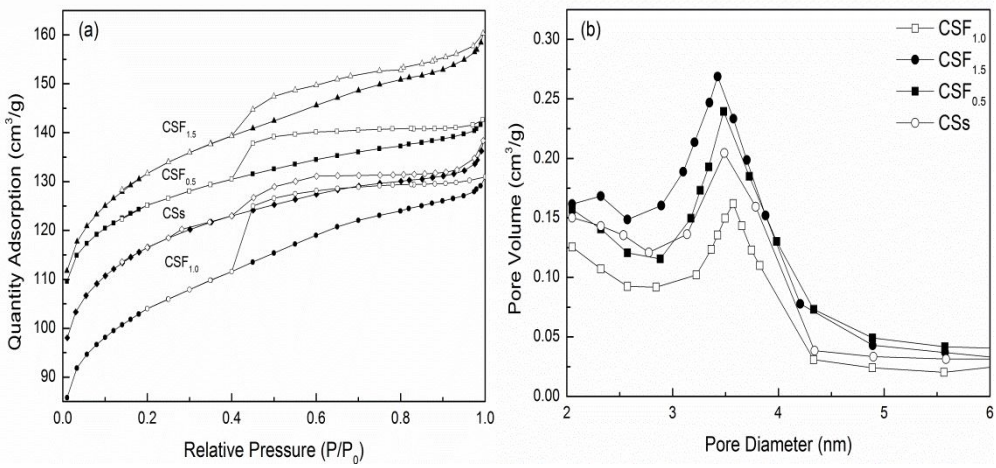

Fig. 2 N_2 adsorption–desorption isotherms and pore diameter distribution of samples prepared with different amounts of F127

Table 1 Textural properties of CSF_n carbonized at different temperatures

Samples	S_{BET} (m^2/g)	S_{mecro} (m^2/g)	S_{micro} (m^2/g)	S_{mecro}/ S_{BET} (%)
$CSF_{0.5}$	385.6	142.4	243.2	36.9
$CSF_{1.0}$	326.2	154.9	171.3	47.5
$CSF_{1.5}$	410.5	123.1	287.4	29.9
CSs	362.9	119.1	243.8	32.8

3.3 ^{13}C solid-state NMR and FTIR analysis

Solid-state ^{13}C was used to confirm the structures of the prepared samples and clarify the function of F127; the spectra are shown in Fig. 3. A preliminary qualitative attribution, based on the literature, was proposed for each spectral domain [36,37]. Region I, between 0 and 100 ppm, is characteristic of sp^3 carbon atoms, indicating the presence of aliphatic and ether carbons. Region II, between 100 and 160 ppm, is characteristic of sp^2-hybridized carbon atoms in C=C double bonds. More specifically, the signals between 100 and 120 ppm arise from O–C=*C* groups within furan moieties [38]. In region III, at 170–250 ppm, the signals represent C=O groups in either carboxylic acid moieties or ketones and aldehydes. On addition of F127, three main changes occur in the spectrum. The peak at 17.9 ppm increases considerably in intensity, indicating that linear

polymerization occurred; this may be caused by bond formation based on hydrophobic groups of F127 (PPO groups) and adjacent reactive functional groups. A clear resonances appears at 105.1 ppm; the data suggest cycloaddition between PEO groups and intermediate products (such as furans, hydroxymethylfurfural, and benzene derivatives), because the peak that appears in region II is typical of aromatic compounds [19,39], confirming that F127 was incorporated into the carbon skeleton structure. Finally, the peaks at 71.9 and 88.9 ppm correspond to residual F127.

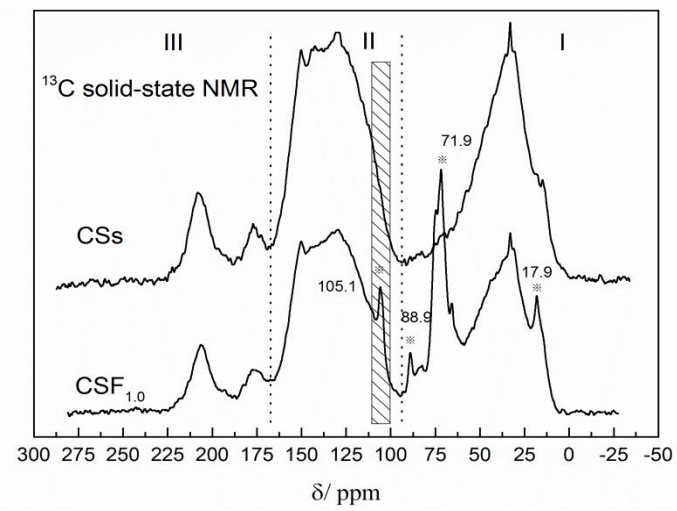

Fig. 3 ^{13}C solid-state NMR spectra of CSs and $CSF_{1.0}$

The FTIR spectra in Fig. 4 show that CSs_{pre} and $CSF_{1.0pre}$ have similar chemical structures. A comparison of the FTIR spectra of the synthesized samples and that of pure CMC shows that new peaks appear during hydrothermal carbonization, indicating that carbon materials rich in functional groups such as hydroxyl, ester, ether carbonyl, and carboxylic groups on the sphere surfaces were obtained [6,7], in good agreement with the solid-state ^{13}C spectroscopic analysis. By comparing the FTIR spectra of the CSs_{pre}, $CSF_{1.0pre}$, and F127, it can be seen that the molecular structure of F127 is largely retained under the hydrothermal conditions, demonstrated by the F127 block copolymer characteristic bands (2885, 1343, 1088, and 840 cm^{-1}) marked in Fig. 4 [40]; these results confirm that F127 was successfully incorporated into the carbon skeletal structure during hydrothermal treatment.

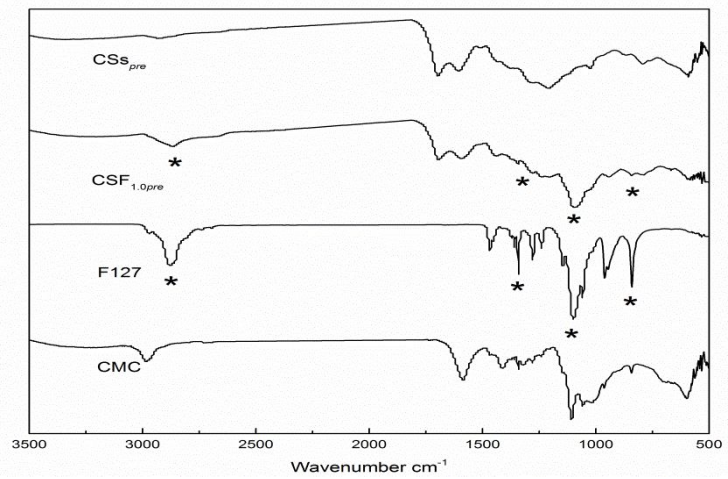

Fig. 4 FTIR spectra of CMC, F127, CSF$_{1.0pre}$, and CSs$_{pre}$

3.4 Thermal analysis

TG and differential TG (DTG) curves of the CSs and CSF$_{1.0}$ are presented in Fig. 5. Both show a small weight loss at low temperature, corresponding to loss of impurities, moisture, and small molecules. Different degradation behavior was observed in the high-temperature range.

Clear losses for the CSs take place in the temperature range of 180–730 °C; this corresponds to the second decomposition stage, with a wide and gradual weight loss, representing nearly 55% loss of the raw materials. In contrast, the degradation of CSF$_{1.0}$ started at a higher temperature and occurred over the temperature range of 230–730 °C. The higher initial degradation temperature can be attributed to reactions between F127 and CMC hydrothermal carbonized intermediate products, confirming that a carbon skeleton with higher thermal stability has been formed. The obvious weight-loss peak at around 380 °C can be attributed to decomposition of F127, and this was complete at 430 °C [41,35]; the remaining carbon skeleton continued to degrade up to 730 °C, the same as in the degradation of CSs.

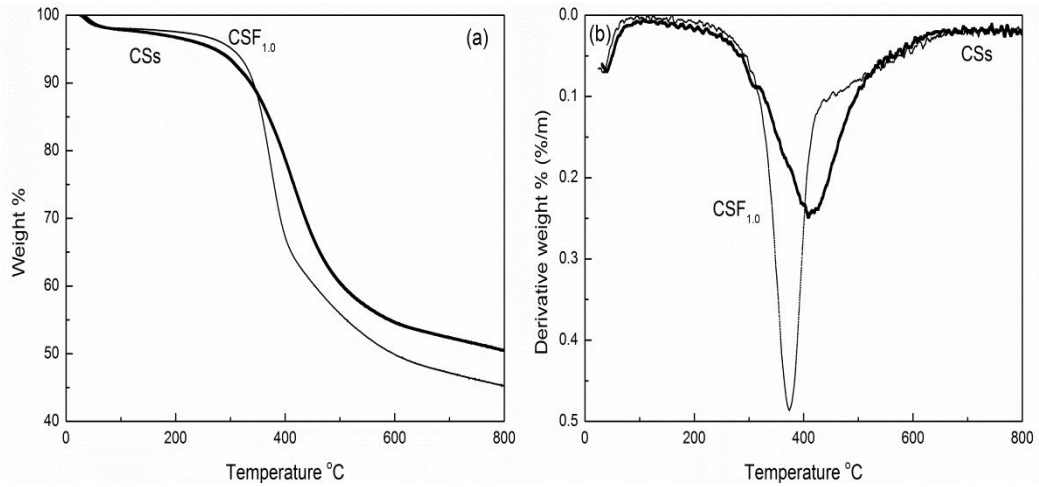

Fig. 5 TG (a) and DTG (b) curves of CSs and $CSF_{1.0}$

3.5 Formation mechanism of flexible cage-like carbon microspheres

Figure 6 shows a schematic of the preparation process. When the CMC is evenly dispersed in F127 solution, the hydrophilic groups of F127 interact with the hydroxyl groups of CMC by hydrogen bonding [18, 42], leading to cross-linking of F127 and the CMC molecular chain. The latter then can be converted to a carbon structure *via* hydrothermal carbonization [6].

At low reaction temperatures and pressures, F127 self-assembles into different states, when the concentration is low, they connect, polymerize, and assemble into amorphous micelles; when F127 reaches the critical micelle-formation concentration (0.7 g), and spherical vesicles are obtained by hydrophilic groups cooperatively self-assembling in aqueous environments [21]. Primary spherical particles with many CMC molecules contained in and around them are formed, and the sizes are determined by the F127 concentration. Larger vesicles with more CMC and encapsulated macromolecules are obtained at higher F127 concentrations.

When the CMC aqueous dispersion is hydrothermally treated at temperature ＞190 °C, CMC chains first hydrolyze to different oligomers and glucose [43], which then undergo dehydration and fragmentation reactions leading to the formation of various soluble products, such as furfural-like compounds, hydroxymethylfurfural-related 1,2,4-benzanetriol and aldehydes [44-45], hydrophilic groups can interact with such intermediate products of CMC hydrothermal treatment (furan and benzene derivatives) *via* cycloaddition to form part of the soluble polymers - the precursor of carbon skeleton, then polymerization or condensation reactions induced by intermolecular dehydration or aldol condensation occurred, leading to the formation of large amount of soluble polymers [46]. The obtained micelles or adjacent primary spherical

nanoparticles formed by F127 were connected after polymerization, linear linking, decarbonylation, and aromatization, *via* active functional groups of CMC intermediate products, reactive macromolecules, with the triblock copolymer F127 synchronous [6,7,25]. At the same time aromatization of polymers takes place, C=O and C=C bonds appear due to the dehydration and the keto-enol tautomerism. When the polymers concentration in the solution reached the critical super-saturation point, a short single nucleation burst occurred with the progress of dehydration and aromatization [47]. Then large spherical aggregates consisting of primary spherical particles are generated and grow constantly by diffusion towards the surface of chemical species present in the solution in an isotropic environment, the driving force for this process is to minimize the surface free-energy of the system and changes in the reaction free-energy [48].

Assembly of the hydrophobic parts as well the reactions between F127 micellar structures and oxygen-containing carbonaceous precursors can contribute to the formation of mesoporous structures [29–32], after carbonization at 800 °C, F127 decomposes completely, leading to opening of the generated pores and condensation of the carbon polymer skeleton, F127 concentration had direct effects on the formation of mesoporous structure, leaving stripe-like 2-D hexagonal mesostructure, cubic mesoporous crystalline structure, disordered worm-like pores, respectively.

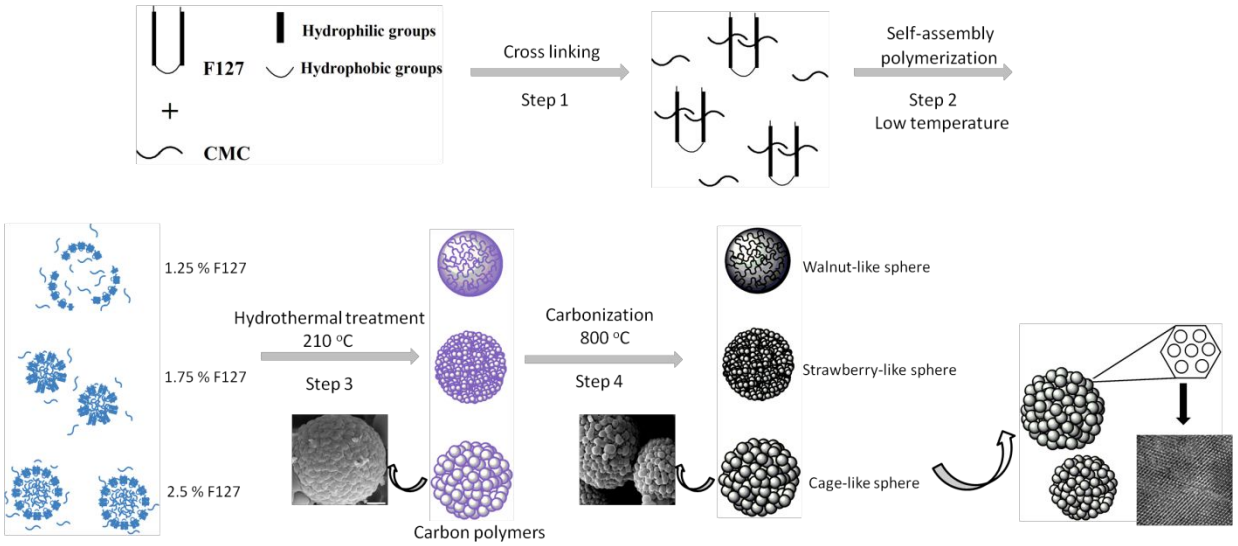

Fig. 6 Formation mechanism of walnut-like, strawberry-like, and cage-like spheres

3.6 Adsorption test of Vitamin B_{12} on different spherical carbon materials

Adsorption capacity for VB_{12} was discussed and shown in Fig. 7, abscissa represents the

concentration of VB_{12} (mg L^{-1}), ordinate represents the adsorption amount of VB_{12} on carbon samples (mg g^{-1}). The results exhibited that all samples show relatively high adsorption capacity for VB_{12}, range from 64 -102 mg/g. VB_{12} are spherical large molecules with diameter of 2.09 nm, they can be effectively adsorbed through the developed mesoporous structure. The mesopores of CSs and CSF_n centered mainly at 3.4-3.6 nm, indicating the VB_{12} molecules can go through and access the interior part of the pores easily.

CSs exhibited adsorption capacity of 64 mg/g, due to the undeveloped and disordered mesoporous structure. Mesoporous ratio increased with the addition of F127, $CSF_{0.5}$ had stripe-like 2-D hexagonal mesostructure, which can contribute to the transportation of VB12 to interior surface, as a result , the adsorption capacity increased. The adsorption isotherms of $CSF_{1.0}$ were of L1 type, because as the VB_{12} concentration increased to a certain value, the adsorption capacity became almost constant, as they consist of 47.5% mesopores, although specific surface area is low, they exhibited highest adsorption capacity of 102 mg/g, besides, the larger and uniform ordered cubic mesoporous can also contribute to the transportation and high adsorption capacity for VB_{12} molecules. For $CSF_{1.5}$, micropores account most proportion, its adsorption capacity decreased, this may due to the pore blockage caused from the aggregation of molecules VB_{12}, which inhibits their further transportation and utilization of interior surface [49].

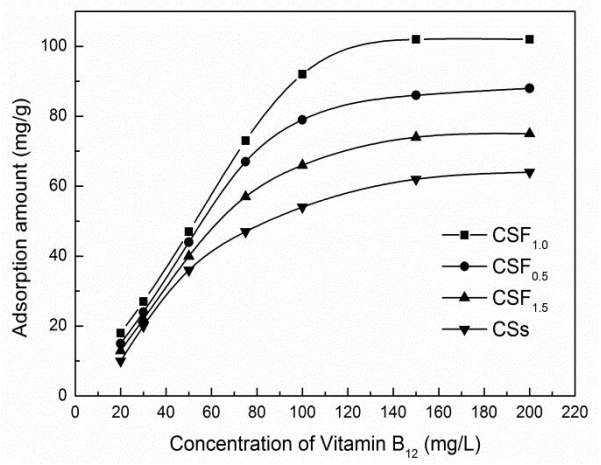

Fig. 7 Adsorption isotherm of $CSF_{0.5}$, $CSF_{1.0}$, $CSF_{1.5}$ and CSs for Vitamin B_{12}

Conclusions

This paper describes a facile tunable synthesis of novel carbon microspheres with different

ordered mesoporous structures and tunable surface morphologies from CMC *via* a soft-template/hydrothermal process. Cooperative self-assembly of F127 forms spherical vesicles that grow and further interact with CMC and the intermediate products of hydrothermal carbonization *via* linear polymerization and cycloaddition. The produced carbon microspheres are transformed from walnut-like, to strawberry-like and cage-like structures when the mass of F127 is increased from 0.5 to 1.0 g. After carbonization, the F127 in the carbon skeleton decomposes, leading to generation of mesopores in the obtained carbon microspheres. The mesoporous percentage and morphology can be controlled well by adjusting the mass of F127, transformed from stripe-like 2-D hexagonal mesostructure to cubic mesoporous to disordered worm-like pores as its concentration increased. Perfect cage-like carbon spheres with a specific surface area of 326.2 m^2/g and a cubic mesoporous structure was obtained for $CSF_{1.0}$, their unique ordered mesoporous structure contributes to the carbon spheres exhibit high adsorption capacity for Vitamin B_{12} of 103 mg/g.

Acknowledgments

This work was financially supported by the Fundamental Research Funds for the Central Universities (2572014EB01), the National Natural Science Foundation of China (No. 31170545), and Project Funded by China Postdoctoral Science Foundation.

References

[1] R. Q. Sun, L. B. Sun, Y. Chun and Q. H. Xu, Carbon, 2008, **46**, 1757.

[2]M. Sevilla, C. Falco, M-M. Titirici and A. B. Fuertes, RSC Adv, 2012, **2**, 12792.

[3] L. Zhao, L. Z. Fan, M. Q. Zhou, H. Guan, S. Y. Qiao, M. Antonietti and M-M. Titirici, Adv. Mater., 2010, **22**, 5202.

[4] S. J. Han, Y. K. Yun, K. W. Park, Y. E. Sung and T. Hyeon, Adv. Mater., 2003, **15**, 1922.

[5] H. Zhang, H. Xu and C. Zhao, Mater. Chem. Phys., 2012, **133**, 429.

[6] M. Sevilla and A. B. Fuertes, Carbon, 2009, **47**, 2281.

[7] X. M. Sun and Y. D. Li, Angew. Chem. Int. Ed., 2004, **43**, 597.

[8] Y. D. Xia and R. Mokaya, Adv. Mater., 2004, **16**, 886.

[9] N. Liu, H. H. Song, X. H. Chen and Y. Wang, Mater. Chem. Phys., 2011, **130**, 1016.

[10] Q. Q. Ke, Y. Q. Liu, H. J. Liu, Y. Zhang, Y. T. Hu and J. Wang, RSC Adv, 2014, **4**, 26398.

[11] Y. Wang, H. H. Song, H. Zhang, L. F. Liao, N. Liu and X. H. Chen, J. Mater. Chem., 2011, **21**, 5576.

[12] Y. Meng, D. Gu, F. Zhang, Y. Shi, H. Yang, Z. Li, C. Yu, B. Tu and D. Y. Zhao, Angew. Chem. Int. Ed., 2005, **44**, 7053.

[13] Y. Fang, D. Gu and R. C. Che, Angew. Chem. Int. Ed., 2010, **49**, 7987.

[14] H. Q. Hu, J. H. Yu, Y. Y. Li, J. Zhao and H. Q. Dong, J Biomed Mater Res Part: A, 2010, **100A**, 141.

[15] J. Lee, S. M. Jin, H. Y. Wang, J. G. Park, H. M. Park and T. Hyeon, Carbon, 2005, **43**, 2536.

[16] S. Kubo, R. J. White, K. Tauer and M-M. Titirici, Chem. Mater, 2013, **25**, 4781.

[17] B. Kelly, G. V. Ricard and M. Daniel, J. Chem. Eng, 2010, **5**, 169.

[18] Z. C. Yang, Y. Zhang, J. H. Kong, S. Y. Wong, X. Li and J. Wang, Chem. Mater., 2013, **25**, 704.

[19] M. Kroger, F. Hartmann and M. Klemm, Chem. Eng.Technol., 2013, **36**, 287.

[20] Y. Matsumura, T. Minowa, B. Potic, S. R. A. Kersten, W. Prins, W. P. M. van Swaaij, B. van de Beld, D. C. Elliott, G. G. Neuenschwander, A. Kruse and M. J. Antal, Biomass Bioenergy, 2005, **29**, 269.

[21] L. Lai, G. Huang, X. Wang and J. Weng, Carbon, 2010, **48**, 3145.

[22] L. Zhang and A. Eisenberg, Science,1996, **272**, 1777.

[23] S. K. Hoekman, A. Broch, and C. Robbins, Energy Fuels, 2011, **25**, 1802.

[24] M-M. Titirici, M. Antonietti and N. Baccile, Green Chemistry, 2008, **10**, 1204.

[25] M. Li, W. Li, and S. X. Liu, J. Mater.Res, 2012, **27**, 1117.

[26] M. Inagaki, H. Orikasa and T. Morishita, RSC Adv, 2011, **1**, 1620.

[27] Y. Meng, D. Gu, F. Q. Zhang, Y. F. Shi, L. Cheng, D. Feng, Z. X. Wu, Z. X. Chen, Y. Wan, A. Stein and D. Y. Zhao, Chem. Mater., 2006, 18, 4447.

[28] Y. Wan, X. F. Qian, N. Q. Jia, Z. Y. Wang, H. X. Li and D. Y. Zhao, Chem. Mater., 2008, 20, 1012.

[29]J. Jin, T. Mitome, Y. Egashira and N. Nishiyama, Colloids and Surfaces A: Physicochmical and Engineering Aspects, 2011, **384**, 58.

[30] K. Kimijima, A. Hayashi and I. Yagi, Chem. Commun , 2008, **44**, 5809.

[31] S.M. Mahurin, J.S. Lee and S.Dai, J. Membr. Sci, 2011, **368**, 41.

[32] M. J. Xie, H. H. Dong, D. D. Zhang, X. F. Guo and W. P. Ding, Carbon, 2011, **49**, 2459.

[33] A. Lu, B. Spliethoff and F. Schuth, Chem Mater, 2008, **20**, 5314.
[34] X. Q. Wang, Q. Zhu and S. Dai, Carbon, 2010, **48**, 557.
[35] C. H. Huang and R. A. Dong, Micropor. Mesopor. Mater 2012, **147**, 47-52.
[36] K. Azami, S. Yamamoto and Y. Sanada, Carbon, 1993, **31**,611.
[37] K. M. Holtman, H. M. Chang, H. Jameel and J. F. Kadla, J. Wood Chem. Technol., 2006, **26**, 21.
[38] N. Baccile, G. Laurent, F. Babonneau and F. Fayon, J. Phys. Chem. C, 2009, **113**, 9644.
[39] R. Demir-Cakan, N. Baccile, M. Antonietti and M-M Titirici, Chem. Mater., 2009, **21**, 484.
[40] Y. Gao , X. H. Wang, H. P. Yang and H. P. Chen, Energy, 2012, **42**, 457.
[41] S. Tanaka, A. Doia, N. Nakatani, Y. Katayama and Y. Miyake, Carbon, 2009, **47**, 2688.
[42] J. Li, X. Ni and K. Leong, Angew. Chem. Int. Ed., 2003, **42**, 69.
[43] Y. Ogihara, Jr. R. L. Smith, H. Inomata and K. Arai, Cellulose, 2005, 12, 595-606
[44] T. M. Aida, Y. Sato, M. Watanabe, K. Tarima, T. Nonaka and H. Hattori, J Supercrit Fluids, 2007, 40, 381-389.
[45] J. N. Chheda, G. W. Huber and J. A. Dumesic, Angew Chem Int Ed, 2007, 46, 7164-7183.
[46] F. S. Asghari, and H. Yoshida, Ind Eng Chem Res, 2006, 45,2163-2173
[47] R. Bacon and M. M. Tang, Carbon, 1964, **2**, 221.
[48] M. Zhang, H. Yang, Y. N. Liu, X. D. Sun, D. K. Zhang and D. F. Xue. Carbon, 2012, **50**, 2155.
[49] X. Zhuang, Y. Wan, C. M. Feng, Y. Shen and D. Y. Zhao. Chem. Mater., 2009, 21, 706.